Plasticity of the xylem vulnerability to embolism in Populus tremula x alba relies on pit quantity properties rather than on pit structure

Cedric Lemaire, Nicole Brunel-Michac, Jérémie Santini, Liliane Berti, Julien Cartailler, Pierre Conchon, Eric Badel, Stéphane Herbette

Research Paper

Plasticity of the xylem vulnerability to embolism in *Populus tremula* x *alba* relies on pit quantity properties rather than on pit structure.

Cédric Lemaire [1], Yann Quilichini [2], Nicole Brunel-Michac [1], Jérémie Santini [2], Liliane Berti [2], Julien Cartailler [1], Pierre Conchon [1], Éric Badel [1] and Stéphane Herbette [1].

[1] Université Clermont Auvergne, INRAE, PIAF, F-63000 Clermont-Ferrand, France.

[2] UMR 6134 SPE, CNRS-Università di Corsica, 20250 Corti, France

Keywords

Acclimation, anatomy, cavitation, hydraulic, phenotypic plasticity, Poplar, shade, water stress, X-ray microCT.

Running head

Structural determinants of plasticity of embolism resistance

Full address of the corresponding author

Stéphane Herbette
UMR INRAE/UCA 547 PIAF
Université Clermont Auvergne, Campus Universitaire des Cézeaux,
1 Impasse Amélie Murat,
TSA 60026, 63178 AUBIERE Cedex
FRANCE
Stephane.Herbette@uca.fr

Abstract

Knowledge on variations of drought resistance traits are needed to predict the potential of trees to acclimate to coming severe drought events. Xylem vulnerability to embolism is a key parameter related to such droughts, and its phenotypic variability relies mainly on environmental plasticity. We investigated the structural determinants controlling the plasticity of vulnerability to embolism, focusing on the key elements involved in the air bubble entry in vessels, especially the inter-vessel pits. Poplar saplings (*Populus tremula x alba*) grown in contrasted water availability or light exposure exhibited differences in vulnerability to embolism (P_{50}) in a range of 0.76 MPa. We then characterized the structural changes in features related to pit quantity and pit structure, from the pit ultrastructure to the organization of xylem vessels, using different microscopy techniques (TEM, SEM, LM). A multispectral combination of X-ray microtomography and light microscopy analysis allowed measuring the vulnerability of each single vessel and testing some of the relationships between structural traits and vulnerability to embolism inside the xylem. The pit ultrastructure did not change, whereas the vessel dimensions increased with vulnerability to embolism and the grouping index and fraction of inter-vessel cell wall both decreased with vulnerability to embolism. These findings hold when comparing between trees, or between the vessels inside the xylem of an individual tree. These results evidenced that plasticity of vulnerability to embolism in hybrid poplar occurs through changes in the pit quantity properties such as pit area and vessel grouping rather than on the pit structure.

Keywords

Acclimation, anatomy, cavitation, hydraulic, phenotypic plasticity, Poplar, shade, water stress, X-ray microCT.

Introduction

According to the cohesion-tension theory (Steudle 2001), the water columns in the xylem are under tension, a metastable state. When this tension increases during droughts, the water columns are more prone to break, because of cavitation: vapour bubbles invade the impacted vessels and spread, impeding function and leading to a loss of xylem conductance. When the loss of conductance reaches a threshold (around 90%), the distal organs are not supplied with water anymore leading to death (Barigah et al. 2013). For woody species, drought-induced death is more likely due to xylem hydraulic failure (Anderegg et al. 2015, 2016, Adams et al. 2017) caused by embolism in the xylem conduits, even if other processes can also contribute to this death (Hammond et al. 2019) such as the carbon starvation (Hartmann et al. 2015).

A global analysis pointed out the narrow hydraulic safety margin at which woody species usually operate (Choat et al. 2012); inferring that research is needed on the variability of vulnerability to embolism. Within-species variability for vulnerability to embolism was shown for many tree species (e.g. Martínez-Vilalta et al. 2009, Herbette et al. 2010). The genetic variability for this trait is rather limited in both natural populations (Lamy et al. 2011, Wortemann et al. 2011) and cultivated species (Jinagool et al. 2015, 2018). This trait would be genetically canalized (Lamy et al. 2012) and varies mainly via plasticity due to environmental factors (Herbette et al. 2010). Plasticity of vulnerability to embolism was reported mainly under water stress, with wood formed under drier conditions being less vulnerable (Awad et al. 2010, Fichot et al. 2010, Plavcová and Hacke 2012). Other conditions such as shade or fertilization were associated to an increase in vulnerability to embolism (Cooke et al. 2005, Barigah et al. 2006, Plavcová and Hacke 2012). However, information is scarce on the determinants of plasticity of vulnerability to embolism. The structural determinants need to be deciphered first, before searching for their genetic control, as it can be complex to decipher the role of candidate genes (Allario et al. 2018).

In angiosperms, water flows between xylem vessels through bordered pits. These pits are openings in the secondary cell wall that allow water to flow between vessels while they prevent air seeding from neighbouring air-filled vessels. Pits have been identified as the key structures for vulnerability to embolism (Lens et al. 2013; Jansen et al. 2018, Kaack et al. 2019). Thus, we assume that the acclimation of vulnerability to embolism to environmental conditions would involve changes in the pit quantity and/or structure, i.e. at pit and/or vessel scales (Lens et al. 2013). The key role of the pit ultrastructure in vulnerability to embolism has been evidenced in several studies (e.g. Choat et al. 2008, Lens et al. 2011, Tixier et al. 2014), especially the pit membrane (Jansen et al. 2009, Li et al. 2016, Kaack et al. 2019). There is a well-established correlation between pit membrane thickness and vessel resistance to embolism in angiosperms (Lens et al. 2011, Plavcová and Hacke 2012, Scholz et al. 2013a, Schuldt et al. 2016). A mechanistic explanation has been provided through the recent discoveries on the three-dimensional structure of the pit membrane (Kaack et al. 2019, 2020). Pit membrane is a porous medium with series of various pore constrictions influencing the air seeding, and constriction sizes decreased with increasing pit membrane thickness. Vulnerability to embolism is also dependent on pit quantity parameters such as the pit area or the vessel connectivity and thus on vessel dimensions and three dimensional organization (Lens et al. 2013). Zimmermann and Jeje (1981) already pointed out that the hydraulic vulnerability could be related to the vessel volume that varies depending on both their diameter (Tyree et al. 1994) and their length (Scholz et al. 2013a). Several studies demonstrated a relationship between vulnerability to embolism and vessel diameter (Wheeler et al. 2005, Hacke et al. 2006, Maherali et al., 2006; Awad et al. 2010, Hajek et al., 2014). However, other studies failed to detect such a relationship (Lens et al., 2011, Scholtz et al. 2013 a, Schuldt et al. 2016). Such discrepancy between findings can be explained by uncertainties about the relationship between vessel diameter and pit area. More, one has to acknowledge that vulnerability to embolism is not controlled exclusively by either pit quantity

parameters or pit structure (Choat and Pittermann 2009). The three-dimensional organization of the xylem network would also influence the vulnerability to embolism, as shown in theoretical and empirical analyses (Loepfe et al. 2007, Mrad et al. 2018). The relationship between vulnerability to embolism and pit properties has been intensively studied at the inter-specific level, whereas the determinants of plasticity of vulnerability to embolism remain poorly investigated at the intraspecific level (Schuldt et al. 2016). For example, in poplar, Plavcová et al. (2011) showed that shading caused an increase in vulnerability to embolism associated with a decrease in both pit membrane thickness and vessel diameter, whereas Awad et al. 2010 showed that a reduced watering induced a decrease in vulnerability to embolism linked with a decrease in vessel diameter.

In this work, we investigated the relationship between the plasticity of vulnerability to embolism and changes in structures related to pit properties at different anatomical levels on young poplars (*Populus tremula x alba*). We grew saplings of a poplar clone under three contrasted environmental conditions for two factors (water and light availability) known to induce variation of vulnerability to embolism. Then, their xylem anatomy was analysed in relation to the changes in vulnerability to embolism using different approaches. Transmission Electron Microscopy (TEM) allowed investigations on the pit ultrastructure. Parameters related to the pit-field were measured using Scanning Electron Microscopy (SEM). We also measured pit quantity parameters related to vessel dimensions and vessel connectivity using light microscopy and silicon injections. Then, an approach using direct observation of embolism spreading inside the xylem by X-ray microtomography allowed to analyse the relationships between structural traits and vulnerability to embolism at the vessel level.

Materials and Methods

Plant material and growth conditions

123 *Plant Material.* Saplings of hybrid poplar (*Populus tremula x alba* clone INRA 717-1B4) were
124 propagated clonally *in vitro* on Murashige and Skoog medium on December 2016. Plantlets
125 were transferred in hydroponic solution on February 2017 and grown in a controlled
126 environment room: 16 h daylight at 21-22 °C, 40 µmol.m^{-2}.s^{-1} and 18-19 °C night, at 70 ± 10 %
127 relative humidity. On March 2017, plants were transferred in 1 Litre pots filled with potting
128 soil (Humustar Terreaux, Champeix, France) with a composition of 25 % brown peat, 40 %
129 blond peat and 35 % pine bark dust. The pots were placed in a greenhouse at the INRAE
130 research station of Clermont-Ferrand, France (site of Crouël; N 45°77′, E 3°14′; 300 m *a.s.l.*).
131 After 20 days, plants were transferred in 10 L pots filled with potting soil. They were regularly
132 watered at soil field capacity. Each pot weighted 6.4 ± 0.4 kg. Ten days later, the specific
133 experimental growth conditions were applied (see next). After one month of growth, stems were
134 cut at 50 cm height. The growth of a new apical bud occurred in May 2017, and any additional
135 bud was removed. Thus, a single stem completely grew under the new environmental
136 conditions.
137 *Experimental setup*. Plants were split in three groups submitted to different growth conditions:
138 (i) “control” plants grew under full sunlight and watered at soil field capacity; (ii) ”droughted”
139 plants grew under full sunlight and watered at 25-30 % of soil field capacity; (iii) ”shaded”
140 plants shaded by a shadehouse that intercepted 30 % of incident light and watered at soil field
141 capacity. For the nine droughted plants, an irrigation at 25-30 % of soil field capacity was kept
142 constant in each pot individually using balances and automatic valves for irrigation as described
143 in Niez et al. (2019). We measured the light interception by the shadehouse by comparing for
144 two months the light intensities recorded with two sensors (PAR/CBE 80, Solems, Palaiseau,
145 France) placed inside the shadehouse and two sensors placed outside. The level of water stress
146 was set to be the most restrictive while allowing growth to produce acclimatized xylem and
147 enough plant material for further analyses. The stem diameter was continuously measured using

a LVDT sensor (Linear Variable Differential Transformer) on three droughted, two control and three shaded plants. Plant height was measured using a measuring tape.

One month before and the day before the tree sampling, predawn water potential (Ψ_{pd}) was measured on every plant 1 hour before the sunrise using a pressure chamber (1505D, PMS Instrument, Albany, OR, USA, Scholender et al. 1965). The same day, midday water potential (Ψ_{mid}) was measured at the solar noon, between 12:00 and 2:00 PM.

Sampling protocol. The sampling was performed on 28 August 2017. Plants were cut at 20 cm height. The plant shoot was immerged underwater and the 30 cm of the top were removed as it lacks significant secondary xylem. Then, the following stem segments were sampled, from basal to apical direction:

i) the 30 cm long basal part of the stem was removed because it was not fully grown under acclimation conditions;

ii) the first 50 cm long of the newly developed stem under the acclimation conditions was wrapped in wet paper, put in a plastic bag and stored at 4 °C until measurements of vulnerability to embolism and vessel length;

iii) the above segment of 6 cm long was devoted to microscopy analyses. It was split into three subsamples using a razor blade: two segments of 1 cm long were prepared for light microscopy and TEM observations. A third segment of 4 cm long was prepared for SEM observations;

iv) if the stem was long enough, an additional segment of 50 cm long was wrapped in wet paper in a plastic bag, and stored at 4 °C for measurements of specific conductivity (K_S) and for additional measurements of vulnerability to embolism;

v) the last 10 cm long was kept wrapped in humid paper for a native embolism measurement performed on the sampling day.

Leaves were sampled under water and the total leaf area (LA) per plant was measured in the day using an area-meter (Li-3100c, Li-Cor Biosciences, Lincoln, NE, USA).

After the sampling, plants were kept in the greenhouse, during the winter 2017. On March 2018, they started growing, still under the same environmental conditions as described above, and on July 2018 we performed a second sample collection: plants were cut at 25 cm height. Then the 30 cm long basal part of the stem was cut underwater. A 50 cm long sample was wrapped in wet paper and stored in a plastic bag at 4 °C for measurements of specific conductivity (K_S).

Hydraulic traits measurements:

Vulnerability to embolism. The 50 cm long stem segment was shortened underwater at 43 cm long using a razor blade. Then, the vulnerability to embolism was assessed using the Cavitron technique (Cochard 2002, Cochard et al. 2005). A centrifugal force increases water tension in branch segment while a specific optical device allows the continuous measurement of the loss of conductance (Cochard et al. 2009). A vulnerability curve was built by plotting the percentage loss xylem conductance (PLC) *vs.* xylem water pressure (P). A sigmoidal function was used to fit each curve using the equation 1 (Pammenter and Willigen 1998).

$$PLC = \frac{100}{1 + e^{\frac{S(P - P_{50})}{25}}} \quad (1)$$

Where P_{50} is the pressure causing 50 % loss of conductance, and S is the slope of the curve at this point.

Specific conductivity. Stem segments of 50 cm long were shortened underwater at a length (L_{stem}) of 40 cm long using a razor blade for droughted (n = 8), control (n = 9) and shaded (n = 9) plants. The apical end of the sample was sealed to a tubing system (polytetrafluoroethylene film) and plugged to an embolism meter (Xyl'em, Bronkhorst, Montigny les Cormeilles, France). The initial conductance (K_i) was then measured under low pressure (2 to 7 kPa) using a solution of 10 mM KCl and 1 mM $CaCl_2$. The xylem area A_X of the distal end of the sample was measured on a cross section using a scanner (V800, Epson, Nagano, Japan). The measurement of A_x was performed on the scanned image using the ImageJ software (version

v.1.52c) (Schneider et al. 2012). The Specific Conductivity K_S was defined according to equation 2.

$$K_S = \frac{K_i \times L_{stem}}{A_x} \qquad (2)$$

Native Embolism. The native embolism of the stem segments of 10 cm long were measured on the sampling day for droughted (n = 9), control (n = 5) and shaded (n = 6) plants. Each sample was shortened underwater using a razor blade to a length of 8 cm. Then, the initial conductance (K_i) was measured under low pressure (2 to 7 kPa) with the same method and the same solution as for specific conductivity. Then, the sample was flushed with the same solution twice for 5 min under high pressure (0.1 to 0.2 MPa) in order to remove the air embolism. A new measurement of conductance without embolism indicated the maximum conductance (K_{max}) of the sample. The native embolism was calculated according to the equation 3.

$$\text{Native Embolism} = \left(1 - \frac{K_i}{K_{max}}\right) \times 100 \qquad (3)$$

Light microscopy

Samples of 1 cm long were cut into 3 x 3 mm^2 blocks then they were immersed in Karnvosky's fixative solution under vacuum for 30 min, then stored at 4 °C in the fixative solution up to the next step. Then, they were dehydrated in an ethanol series (50, 70, 80, and 95 %) and embedded in LR White resin. Transverse slices of 2 to 3 µm thick were cut using an ultramicrotome (Om U2, Reichert, Vienna, Austria). Sections were stained with 1 % (w/v) toluidine blue, washed 4 times with water and mounted in Eukitt (Sigma-Alrich, St-Louis, MO, USA). Images were processed using a microscope (Zeiss Axio Observer Z1), a digital camera (AxioCam MRc) and Zen imaging software system (Zeiss, Jena, Germany).

Image analyses were performed using ImageJ software with a home-made semi-automated procedure. The vessel diameter (D_v) was estimated to be the diameter of the circle having the same area as the vessel lumen (for the symbols, see Table 1). The total vessel wall perimeter in contact with other vessel was measured using the Feret diameters. The vessel diameters were

increased by five pixels using dilate function and if dilated vessels overlapped, they were considered to be in contact. The maximum Feret diameter of the overlapping area was considered to be their length of wall in contact. From there, the contact fraction (F_c) was measured for each vessel as the ratio of length of wall in contact with other vessels over the perimeter of the vessel. Vessels that shared wall were assigned to the same group. As a result, the two-dimensional grouping index (GI) was the mean number of vessels per group and the solitary index (SI) as the ratio of the number of solitary vessels to the total number of vessels. These parameters were measured for each individual slice containing a mean of 850 vessels, for droughted (n = 9), control (n = 5) and shaded (n = 6) plants.

Vessel length

The vessel length was measured by the silicon injection method (Sperry et al. 2005, Scholz et al. 2013b) on the samples already used for Cavitron technique, after five months of drying at room temperature. A fluorescent optical brightener (CAS number: 7128-64-5, Sigma-Aldrich, St-Louis, MO, USA) was mixed in chloroform (1 % w/w) and added to a volume of silicon (BLUESIL RTV-141 A, Bluestar Silicones, Lyon, France) with a proportion of one drop of solution per gram of silicon. A Silicone hardener (BLUESIL RTV-141 B, Bluestar Silicones) was added to the mixture in 1:10 proportion. The mixture was then injected under pressure (300 to 400 kPa) basipetally in the stem sample using a pressure chamber during at least 8 hours. After silicone hardening (3 days at room temperature), the samples were cut 5 mm far from the injection point; then every 20 mm. For each segment, a 25 µm thick slice was cut using a rotary microtome (RM2165, Leica Microsystems, Wetzlar, Germany). Cross sections were dyed with Astra Blue and mounted with a glycerol medium.

Images were obtained using a fluorescence microscope (Axio Observer Z1) equipped with a 300 to 400 nm band pass excitation filter, a digital camera (AxioCam 506), Zen imaging software system (Zeiss, Jena, Germany) and analysed using the ImageJ software. Fluorescent

vessels highlighted the open vessels, while white light allowed counting the total number of vessels. The decrease of the ratio of open vessels (N_x) (*i.e.* fluorescent vessels) to the total number of vessels (N_0) over the distance (x) from the end of the sample followed an exponential decay function (equation 4) where k is the best-fit extinction coefficient (Cohen et al. 2003).

$$N_x = N_0 \times e^{-kx} \quad (4)$$

The fraction of conduits of length x ($P(x)$) is obtained by multiplying x/N_0 to the second derivative of equation 4 (Wheeler et al. 2005):

$$P(x) = x \times k^2 \times e^{-kx} \quad (5)$$

The continuous cumulative function of vessel length (Lv) probability is a function given in the equation 6.

$$f(x) = \int_0^{L_v} x k^2 . e^{-kx} \mathrm{d}x \quad (6)$$

When this cumulative function is equal to 0.5, this gives the median value of vessel length (L_v) (equation 7).

$$f(L_v) = -(kL_v + 1).e^{-kL_v} + 1 = 0.5 \quad (7)$$

The solution of the equation 7 gives the median vessel length $L_v = 1.678/k$. This vessel length was estimated for 7 droughted, 5 control and 5 shaded stem samples.

Transmission Electron Microscopy

Fresh samples of 1 cm long were cut into 2 to 4 mm^3 blocks, immersed in Karnvosky's fixative solution under vacuum for 30 min, then stored at 4 °C in the fixative solution for 3 weeks. Blocks were recut into 1 to 2 mm^3 pieces, then they were fixed secondarily for 4 hours at ambient temperature in a 0.1M phosphate-buffered osmium tetroxide solution (1 %), pH 7.4. Then, they were dehydrated in an ethanol series (25, 50, 70, 100, and 100 %) and embedded in Epoxy resin using Epoxy medium kit (Sigma-Aldrich, St-Louis, MO, USA). Then, ultra-thin sections (60-90 nm) were cut using an ultramicrotome (PowerTome PC, RMC Boeckeler, Tucson, AZ, USA). The sections were placed on 200- and 300-mesh copper grids and stained

with contrast solutions: UranyLess (Delta Microscopies, Mauressac, France) and lead citrate. Sections were observed using a transmission electron microscope (H-7650, Hitachi High-Technologies Corporation, Tokyo, Japan) at a voltage of 80 kV. Measurements of pit features were performed on images with pits showing two apertures. Pits were characterized for their diameter (D_p), their aperture diameter (D_a), their chamber depth (L_p) and their membrane thickness (T_m). For each pit, D_a was the mean of two measurements while L_p and T_m were the mean of four measurements. Pit features were measured for five individual trees for each growth condition, with at least 10 pits measured per individual tree.

Scanning Electron Microscopy

Fresh samples were fixed in 3 % glutaraldehyde and stored at 4 °C for at least 1 month. Samples of 4 cm long were cut longitudinally and then dehydrated in an ethanol series (30, 50, 75, and 100 %). After dehydration, samples were immerged in a 1:1 solution hexamethyldisilazane (HMDS) + ethanol 100 % for 30 min and immerged in pure HDMS for 30 min. After air drying overnight under a hood, the samples were mounted on aluminium stubs with carbon double-sided adhesive disks, coated with gold/palladium in a sputter coater (SC7640, Quorum Technologies Ltd, Newhaven, U.K.), and finally observed using a scanning electron microscope (S-3400N, Hitachi High-Technologies Corporation, Tokyo, Japan) at a voltage of 5 kV. The portion of area covered by bordered pits in each inter-vessel pit-field (F_{pf}) was then measured by image analysis using the ImageJ software. Five samples were measured per growth condition, and seven pit-fields were characterized per sample.

Estimation of supplementary hydraulic and structural traits

Theoretical conductivities (K_{s_theo}) of all samples characterized by light microscopy were calculated according to Scholz et al. (2013b) and converted into $g.s^{-1}.MPa^{-1}.m^{-1}$ (equation 8).

$$K_{s\_theo} = \frac{\sum \frac{\pi D_v^4}{128\,\eta}}{A_x} \times \rho \qquad (8)$$

Where η is the viscosity index of water (1.002×10^{-9} $m^4.MPa^{-1}.s^{-1}$ at 20 °C), ρ is the density of water (9.982×10^5 $g.m^{-3}$) and A_x is the xylem cross-section area.

The pit fraction (F_p) was defined as the product of the pit-field fraction (F_{pf}) and the contact fraction (F_c) (equation 9).

$$F_p = F_{pf} \times F_c \qquad (9)$$

The pit fraction was measured on five individual trees for each growth condition.

The vessel area (A_v) was estimated as the area of a cylinder according to the equation 10.

$$A_v = D_v \times L_v \times \pi + 2\pi\left(\frac{D_v}{2}\right)^2 \qquad (10)$$

It was measured for 7 droughted, 5 control and 5 shaded trees.

The pit area per vessel (A_p) was calculated as the product of the vessel area A_v by pit fraction F_p (equation 11).

$$A_p = A_v \times F_p \qquad (11)$$

It was measured for 4 droughted, 5 control and 4 shaded individuals.

Xylem water potentials at the onset of xylem embolism (P_{12}) and at full embolism (P_{88}) were calculated using equation 12 and 13 respectively (Domec and Gartner 2001), using the experimental values of P_{50} and S resulting from equation 1.

$$P_{12} = P_{50} + \frac{50}{S} \qquad (12)$$

$$P_{88} = P_{50} - \frac{50}{S} \qquad (13)$$

Measurement of individual vessel vulnerability to embolism using multispectral approach combining X-ray microtomography and light microscopy

Two stem segments from droughted plants and two from control plants were sampled and prepared in the same condition as for vulnerability to embolism measurements. We used the techniques described in Cochard et al. (2015). Segments were shortened underwater at 34 cm

long using a razor blade, sealed in liquid paraffin wax in order to prevent dehydration during the microtomography scans. A first 21 min scan was acquired using a X-ray microtomography system (Phoenix Nanotom, General Electric, Boston, MA, USA) at the centre of the segment as described below to reveal the native state of embolism in each shoot. The field-of view was $7.8 \times 7.8 \times 7.8$ mm^3 and covered each full cross section of the samples. X-ray source settings were 60 kV and 240 µA. 1000 images were recorded during the 360 ° rotation of the sample and the final spatial resolution was 3.9 µm.

Then, the paraffin was broken at the ends in order to allow the water flow and the sample was set in a Cavitron during 5 min at 0.8 MPa, immerged in paraffin and scanned again with the X-ray microtomograph at the same location than previously in order to observe the new embolism status. The same procedure was repeated for increasing pressure steps, until - 4 MPa (Fig. 1).

Then, the stem sample was cut in the air at 5 mm above the scanned section in order to generate 100 % of embolism of the functional vessels and a last microtomographic scan was performed in order to visualize this complete vessel network.

The sample was then dried several days in room conditions and a transverse section of 25 µm thick was cut with a rotary microtome (RM2165, Leica Microsystems). Sections were dyed with series of baths as following: bleach (about 15 sec), acetic acid, Astra blue (1 min), acetic acid, safranin (1 min), acetic acid with a water bath between each solution, then an ethanol series (50, 70, 100 and 100 %). The sections were mounted in Eukitt. Images were processed using a microscope (Zeiss Axio Observer Z1), a digital camera (AxioCam MRc) and Zen imaging software system (Zeiss, Jena, Germany). Image analyses were performed using Fiji software (under ImageJ version 2.0.0-rc-68/1.52h) (Schindelin et al. 2012, Schneider et al. 2012), using the same method described in the section for light microscopy. The diameter of each vessel (D_v^*) was estimated as the diameter of the circle that provided the same area as the vessel lumen. For each vessel, the number of vessels in the group (Group Size; GS) and the

fraction of membrane in contact with other vessels (F_c^*) were also estimated on the cross-section plane. Finally, the relative distance from the pith was measured for each vessel as the ratio of the distance from the pith to the vessel over the distance from the pith to the cambium. The microtomography scans were reconstructed in three-dimension (3D) using Phoenix datosx 2 software (General Electric, Boston, MA, USA) with spatial resolution of 6.8 × 6.8 × 6.8 µm^3 per voxel. Then, for each 3D-reconstruction, a cross section was extracted at the exact same location as with the microscopy section. For each vessel in the cross sections, its embolism pressure (P_e) is defined as being the centrifugation-induced pressure from which the vessel appeared to be air-filled on microtomographic images (Fig. 1, A-D).

For each sample, images from x-ray microtomography observation (virtual cross sections built by 3D reconstruction) were aligned on the light microscopy image (stem cross section observed by light microscopy) using the "Align image by line ROI" tool (Schindelin et al. 2012) of Fiji software. A unique identification number was given to each vessel observed in images from both techniques, in order to link the embolism pressure with anatomical parameters (Fig. 1, E). A total of 2570 vessels were identified. Vessels were grouped per D_v^*, per F_c^* and per GS classes. Classes were sized to be as uniform as possible, counting from 183 up to 748 vessels. A total of 1100 solitary vessels were grouped in the same class when required. Cumulative number of embolized vessels was plotted according to their P_e and, for each class, a Weibull function was fit (equation 1).

Statistical analysis

The statistical analysis was performed using the RStudio software (version 1.1.456; running under R core version 3.5.1, R Development Core Team 2008). One way ANOVA was used for comparing the means between the three growth conditions. When we found a significant difference, we referred to Tukey's multiple range test at $p < 0.05$ to compare the mean values

between growth conditions. The correlations between the structural traits and the P_{50} and P_e were calculated using linear regressions.

Results

Continuous recordings of the radial growth showed a significant lower growth for the droughted plants throughout the experiment (Fig. S2, Table 2). These plants also showed a lower height, lower leaf area, lower Ψ_{pd} and lower Ψ_{md}, demonstrating the significant effect of our drought treatment. The higher leaf area for shaded plants compared to control plants is an evidence that the shading conditions affected the plant development.

Growing plants under different environmental conditions aimed to induce wide variations in xylem vulnerability to embolism. The three growth conditions spread the measured P_{50} over range from - 2.00 to - 3.47 MPa (Table S1), with a difference of 1.04 MPa between the most resistant droughted plant and the most vulnerable control plant and a difference of 1.47 MPa between the most resistant droughted plant and the most vulnerable shaded plant. A significantly lower P_{50} was found on droughted plants when compared to control and shaded plants ($p < 0.001$, Table 2), while the slopes of the vulnerability curves were not different between the growth conditions (Fig. 2, A). Despite a slightly higher native embolism for droughted plants compared to shaded plants, Ψ_{mid} was higher than the inflexion point of the vulnerability curve (P_{12}) for every growth conditions. This allows excluding any effect of these quite low native embolism on measured P_{50}. We observed no difference for mean K_S between the growth conditions (Fig. 2, B), suggesting no plasticity for this trait in our experimental conditions. When considering the vessel diameter, a reduced K_{s_theo} was measured in the droughted plants compared to control and shaded plants (Table 2).

The analyses combining different methods (light microscopy, TEM, SEM), allowed measuring a large set of anatomical traits from tissue to pit levels. The correlation between these traits and the P_{50} was assessed (Fig. 3, 4).

The traits measured at tissue level (GI, SI and F_p) showed a strong linear correlation with P_{50} ($R^2 > 0.70$; $p < 0.001$; Fig. 3, 4), except F_c that exhibited a weaker correlation ($R^2 = 0.38$; $p = 0.004$). These results put in light a relationship between vessel connectivity, vessel grouping and vulnerability to embolism (negative relationship for F_c, GI and F_p; positive relationship for SI). However, we found no correlation between pit-field fraction (F_{pf}) and P_{50}, with no variation among the growth conditions (Table 3). We observed a strong positive relationship ($p < 0.001$) between P_{50} and the vessel dimensions (L_v, D_v and A_v) showing that larger vessels with larger pit area tend to be associated with an increase in vulnerability to embolism ($R^2 > 0.75$; $p < 0.001$). The positive correlation between P_{50} and A_p ($R^2 = 0.78$; $p < 0.001$, Fig. 4) highlighted the link between the area of vessels covered by bordered pits and the xylem vulnerability to embolism.

No linear correlation appeared between the pit structure parameters (D_a, D_p, L_p and T_m) and the P_{50}: we observed no variation for D_a, D_p and T_m among growth conditions.

Using x-ray microtomograph, the direct visualization of embolism inside the xylem (Fig. 1) allowed evaluating the vulnerability to embolism (P_e) of individual vessels. The multispectral analysis combining x-ray tomographic observations and the measurements made on light microscopy images allowed establishing the link between P_e and the structural parameters of each vessel (Fig. 5). The correlation between D_v^* and P_e (Fig. 5, A) was clear: wider vessels appeared more vulnerable than the narrower ones. F_c^* showed a smaller influence on P_e (Fig. 5, B): solitary vessels ($F_c^* \leq 1$ %) and weakly connected vessels ($1 < F_c^* \leq 20$ %) were more vulnerable than the highly connected vessels ($F_c^* > 20$ %). The link between GS and P_e (Fig. 5, C) appeared to be the less clear: the most vulnerable vessels were the solitary ones whereas the

grouped vessels ($GS \geq 2$) were less vulnerable. Despite a significant correlation between P_e and D_v^*, F_c^* and GS ($p < 0.001$; Fig. 6), the strength of the correlation was poor ($R^2 < 0.25$). We also noticed that the position of the vessel in the cross section is linked to its vulnerability (Fig 1): the more the vessels were far from the pith, the more they were more resistant to embolism. ($R^2 = 0.49$; $p < 0.001$; Fig. 5, D; Fig. 6).

Discussion

The range for P_{50} plasticity induced by the growth conditions was large: 0.76 MPa between the mean P_{50} of droughted and shaded plants (Table 2; Fig. 2, A) and up to 1.47 MPa between two individuals. This is consistent with previous studies: Awad et al. (2010) reported a difference of 0.63 MPa between droughted and well-watered plants; Plavcová and Hacke (2012) reported a difference of 1.08 MPa between droughted and shaded *Populus trichocarpa x deltoides* plants. Therefore, the plasticity induced by our experimental setup was probably close to the maximum we could expect according to the literature.

The absence of difference in specific hydraulic conductivity (K_s) between droughted and control plants (Table 2; Fig. 2, B) was consistent with the results of Gleason et al. (2016): who reported a poor correlation between vulnerability to embolism and K_s in their meta-analysis. Furthermore, the lack of trade-off between hydraulic efficiency and safety was also observed within species (Awad et al. 2010, Plavcová and Hacke 2012, Schuldt et al. 2016). A significant decrease of the theoretical conductivities (K_{s_theo}) was found for droughted plants compared to other plants (Table 2), relying on a decrease in vessel diameter (D_v) (Table 3); whereas the pit structure was not modified (Table 3). However, This theoretical decrease in lumen conductance in droughted plants is only based on the Poiseuille's law and could be offset by other changes we did not investigate, such as three-dimensional xylem organization, vessel wall sculpturing, pit biochemistry or pit membrane porosity.

442 P_{50} was correlated with anatomical traits related to pit quantity characteristics measured at the
443 xylem and vessel levels (significant correlations with $R^2 > 0.7$ for 7 out of the 9 traits; Fig. 3,
444 4). These pit quantity parameters were correlated between them, which is not very surprising
445 since they all measure slightly different features of vessel connectivity (Table S2; Fig. S3).
446 Indeed, such correlations were also found when comparing *Acer* species (Lens et al. 2011). By
447 contrast, no correlation was found with the traits related to the pit dimensions (D_a, D_p, L_p and
448 T_m; Fig. 3). Thus, the pit ultrastructure does not appear as a driver of the plasticity of
449 vulnerability to embolism in *Populus tremula x alba* (Fig. S1). Despite a key role of T_m in
450 determining vulnerability to embolism, the air-seeding pressures for thin pit membrane such as
451 those of poplar xylem would not be influenced by slight changes in its thickness (Li et al. 2016,
452 Kaack et al. 2019). So, the role of pit structure in plasticity of vulnerability to embolism remains
453 to be tested in species having much thicker intervessel pit membranes. The observation of a
454 variation in vessel diameter not associated with a variation in pit membrane thickness is not
455 surprising, since this has already been reported when comparing the anatomy between organs
456 along the flow path in several species of angiosperm (Klepsch et al. 2018). Other relevant pit
457 parameters could also be considered, but suitable methods for investigating their variability are
458 lacking. For example, the pit membrane porosity contributes to the differences in vulnerability
459 to embolism (Jansen et al. 2009, Li et al. 2016, Kaack et al. 2019); but this parameter is difficult
460 to measure accurately because pores include a series of various pore constrictions, and the
461 narrowest constriction should be the main bottleneck (Kaack et al. 2019, Kaack et al. 2020,
462 Zhang et al. 2020). The role of the biochemical composition of the pit membrane in the
463 plasticity of vulnerability to embolism cannot be excluded too. Besides, there have been recent
464 advances in the understanding of the pit membrane biochemistry, including a role for lipids
465 (Herbette et al. 2015, Klepsch et al. 2016, Schenk et al. 2017, Pereira et al. 2018, Schenk et al.
466 2018, Kaack et al. 2019). Moreover, calcium in pit membrane was reported to be a major

467 determinant of between-species differences in vulnerability to embolism, but it was not
468 involved in the plasticity of vulnerability to embolism (Herbette and Cochard 2010).

469 At the interspecific level, pit ultrastructure parameters, especially the pit membrane thickness,
470 was identified as the major traits involved in variation in vulnerability to embolism (Jansen et
471 al. 2009; Tixier et al. 2014, Li et al. 2016, Kaack et al. 2019). In addition, between species
472 differences in vulnerability to embolism also depend on pit mechanical behaviour (Tixier et al.
473 2014). The probability for air seeding through large pores is expected to be higher when more
474 pits are present (rare pit hypothesis proposed by Christman et al. 2009). The pit area can thus
475 explain differences in vulnerability to embolism for some angiosperm groups but not for others
476 (Lens et al. 2013). Thus, when explaining the variability in vulnerability to embolism between
477 species, this trait, which depends on the vessel dimensions and xylem organization, does not
478 appear very relevant (Lens et al. 2013). Lens et al. (2011) tested the relationship between several
479 pit quantity and pit structure properties and vulnerability to embolism for 11 acer species. They
480 found that vulnerability to embolism strongly correlated with depth of bordered pit chamber
481 (L_p) and pit membrane thickness (T_m) whereas no relationship was found between vulnerability
482 to embolism and vessel diameter (D_v) and total pit area per vessel (A_p). By contrast, our results
483 suggest that the plasticity of vulnerability to embolism in poplar is controlled by the xylem
484 organization and vessel dimensions, and not by changes in pit structure. Thus, the mechanisms
485 controlling the inter-specific variability in vulnerability to embolism seem to be different from
486 the drivers of the within species plasticity in poplar. Complementary works on plasticity need
487 to be carried out on other species, particularly on species with much thicker pit membranes, in
488 order to test the genericity of the findings of this study. It would not be surprising if the
489 mechanisms of plasticity could be different depending on the species. A recent modelling
490 analysis of the relationships between the functional and structural pit properties provides some
491 interesting insights agreeing with our results and supporting different mechanisms for plasticity

(Kaack et al. 2020). According to this analysis considering the internal structure of the pit membrane, three functional types of pit can be distinguished based on their T_m : (1) a pit with a thin T_m (< 150 nm) would have large pores causing a low embolism resistance not very sensitive to the pit area, (2) a pit with a thick T_m (>400 nm) with narrow pores allowing high embolism resistance insensitive to the pit area and (3) an intermediate pit membrane type, with embolism resistance strongly affected by the pit area. This latter type includes the case we studied and thus it agrees well with our results. Indeed, the model predicts that the vulnerability to embolism is strongly affected by the pit area for vessels with a pit membrane thickness of 250 nm.

The multispectral analysis combining X-ray microtomography analysis with light microscopy revealed that P_e shows the strongest correlation with the position of the vessel relative to the pith (Fig. 6). However, significant correlations were also found between the others xylem traits (D_v, F_c and GS) and this radial position ($p < 0.001$), so no clear conclusion can be drawn about an effect of vessel age or position on its vulnerability to embolism. The stem fully developed in 3 months, and much less for the secondary xylem of the stem part investigated by X-ray microtomography. We thus assume that the age difference is too weak to explain such difference in vulnerability to embolism. Indeed, in diffuse-porous species, an age effect in vulnerability to embolism has been reported between vessels formed in different years but not between vessels of the same year (Melcher et al. 2003). Moreover, investigations of the embolism spread in current-year stem of vine or walnut tree using the same approach did not conclude to an age effect in the secondary xylem (Brodersen et al. 2013, Knipfer et al. 2015). These two previous studies showed that embolisms formed first in vessels surrounding the pith, then they spreaded overwhelmingly radially while the water potential was decreasing. The sequence of embolism formation and spreading in our study could therefore be related to the mechanism explained by Brodersen et al. (2013). More, we also hypothesize that vulnerability to embolism decreased during development in relation to changing water conditions *in planta*.

517 Although the soil moisture content was kept constant, the midday water potential of the plant
518 decreased as the plant grew (Table 2). The pressure inducing embolism being correlated with
519 the midday water potential experienced by plants (Awad et al. 2010), the acclimation of
520 vulnerability to embolism would occur during the development of plants.
521 Vulnerability curves are commonly established by measuring the impact of embolism on the
522 conductance, but not the embolism rates. Thus, "hydraulic vulnerability" is a more suitable term
523 when comparing xylems for P_{50} using these methods. Conversely, X-ray microtomography
524 methods really allow assessing the local vulnerability to embolism.
525 Our results showing a strong relationship between P_{50} and some vessel and xylem tissue
526 parameters provide three non-exclusive explanations for the acclimation of hydraulic
527 vulnerability. This latter relies on changes in vulnerability to embolism of the vessels or on
528 changes in the effect of the embolism on conductance. First, our study shows that vulnerable
529 individuals exhibited larger vessels (both longer (L_v) and wider (D_v); Fig. 3). When a large
530 vessel embolizes, it generates a greater impact on the hydraulic conductivity compared to a
531 smaller vessel. Thus, a xylem having a high proportion of large vessels undergoes an important
532 drop of conductivity after each vessel embolism. Second, we found that vulnerable xylems had
533 a greater SI and a lower GI and F_c. Redundancy in the xylem has already been linked with a
534 lower hydraulic vulnerability using a modelling approach (Ewers et al. 2007, Mrad et al. 2018).
535 High connectivity and grouping is an efficient way to maintain the hydraulic conductance
536 despite embolized vessels in the xylem by providing alternative pathways to the water flow
537 (Carlquist 1966, Schuldt et al. 2016). Third, larger vessels have a larger pit area per vessel (A_p)
538 and would thus be more prone to embolism, according to the pit area hypothesis (Christman et
539 al. 2009). Multispectral analysis combining X-ray microtomography and light microscopy
540 allowed monitoring the dynamics of xylem embolism and in particular determining the
541 embolism pressure of each vessel (Fig.1; Fig. 5). This approach supports the third explanation,

since larger vessels (D_v^*) showed a higher vulnerability to embolism– as noticed by Cai and Tyree (2010) using a statistical, indirect and destructive technique and by Jacobsen et al. (2019) using a similar approach. Nevertheless, the poor correlations (low R^2 values) between the embolism pressure of each vessel (P_e) and D_v^*, F_c^* or GS suggest that the rare pit hypothesis is far from being sufficient for explaining the hydraulic vulnerability inside a stem sample. According to Kaack et al. (2019), the rare pit hypothesis is not compatible with the three dimensional structure of the pit. Other additional mechanisms could be involved to explain the plasticity of hydraulic vulnerability observed among growth conditions: they would include the effect of redundancy and of vessel embolized volume on the loss of conductance, or change in pore constrictions in pit membranes. That is why we assume that the different mechanisms we described here act together to design the hydraulic vulnerability during acclimation. The lowest correlations found between P_e and F_c^* or GS point to the limitations of a bi-dimensional approach to analyse vessel connectivity. Some studies reported analyses of the three-dimensional xylem network (Brodersen et al. 2011), that allowed investigating events of embolism formation and spreading (Brodersen et al. 2013, Knipfer et al. 2015, 2016, Torres et al. 2016). Rather short segments (2-6 mm long) were examined what was enough for their study. The vessels having an average length of about ten cm (up to 30 cm), would require analysis of the vessel organization over a longer sample length for a full quantification of their connectivity. This was impossible with the x-ray microtomograph device we used. Moreover, such a large volume of wood could not be scanned without a very high temperature increase to maintain sufficient resolution.

In conclusion, we found that the acclimation of vulnerability to embolism to contrasted growth conditions in hybrid poplar did not rely on a change in pit ultrastructure, contrary to what was reported when comparing species. Thus, within-species plasticity in hybrid poplar and between-species variability for vulnerability to embolism could rely on different mechanisms. We

showed that an increase in resistance to embolism in poplar is related to an increase in vessels connectivity and grouping and a decrease in vessel dimensions, leading to reduce the likelihood of air seeding through a pit and the effect the resulting embolism events on hydraulic conductance. This study will allow focusing on the relevant candidate genes controlling vulnerability to embolism such as those involved in vessels grouping and connectivity or vessel dimensions. These genes include the aquaporins involved in cell expansion during xylogenesis (Plavcová et al. 2013), the genes controlling the cell wall metabolism in xylem such as *VND6*, *VND7* and *MYB46*, which expression levels changed in response to an abiotic stress (Plavcová et al. 2013, Taylor-Teeples et al. 2016) or *CLE* genes (*CLE41* and *CLE44*) that repress the xylem differentiation (De Rybel et al. 2016).

Funding

This work was supported by European Union within the context of European Regional Development Fund (ERDF).

Acknowledgements

The authors thank Christelle Boisselet and Brigitte Girard for the plant production, Christophe Serre for the LDVT preparation, Romain Souchal for the balances and LVDT set up, Patrice Chaleil, Aline Faure and Stephane Ploquin for growing the plants in the greenhouse, André Marquier for the PAR measurements and Felix Hartmann for his help in calculating the vessel length. The authors also thank the PhenoBois plateform for the X-ray microtomography facility.

Authors' contributions

C.L. and S.H. designed the study and wrote the manuscript with contributions from all authors. C.L., S.H., P.C. and J.C. performed field work and hydraulic measurements; C.L., N.B-M., Y.Q., L.B. and J.S. performed electron microscopy; C.L., N.B-M., P.C. performed light

591 microscopy; C.L., P.C. and E.B. performed X-ray microCT; C.L., P.C. and E.B. performed
592 image analysis. All authors approved this manuscript.

References

Adams HD, Zeppel MJB, Anderegg WRL, Hartmann H, Landhäusser SM, Tissue DT, Huxman TE, Hudson PJ, Franz TE, Allen CD, Anderegg LDL, Barron-Gafford GA, Beerling DJ, Breshears DD, Brodribb TJ, Bugmann H, Cobb RC, Collins AD, Dickman LT, Duan H, Ewers BE, Galiano L, Galvez DA, Garcia-Forner N, Gaylord ML, Germino MJ, Gessler A, Hacke UG, Hakamada R, Hector A, Jenkins MW, Kane JM, Kolb TE, Law DJ, Lewis JD, Limousin J-M, Love DM, Macalady AK, Martínez-Vilalta J, Mencuccini M, Mitchell PJ, Muss JD, O'Brien MJ, O'Grady AP, Pangle RE, Pinkard EA, Piper FI, Plaut JA, Pockman WT, Quirk J, Reinhardt K, Ripullone F, Ryan MG, Sala A, Sevanto S, Sperry JS, Vargas R, Vennetier M, Way DA, Xu C, Yepez EA, McDowell NG (2017) A multi-species synthesis of physiological mechanisms in drought-induced tree mortality. Nat Ecol Evol 1:1285–1291.

Allario T, Tixier A, Awad H, Lemaire C, Brunel N, Badel É, Barigah TS, Julien J-L, Peyret P, Mellerowicz EJ, Cochard H, Herbette S (2018) PtxtPME1 and homogalacturonans influence xylem hydraulic properties in poplar. Physiol Plant 163:502–515.

Anderegg WRL, Flint A, Huang C, Flint L, Berry JA, Davis FW, Sperry JS, Field CB (2015) Tree mortality predicted from drought-induced vascular damage. Nature Geosci 8:367–371.

Anderegg WRL, Klein T, Bartlett M, Sack L, Pellegrini AFA, Choat B, Jansen S (2016) Meta-analysis reveals that hydraulic traits explain cross-species patterns of drought-induced tree mortality across the globe. PNAS 113:5024–5029.

Awad H, Barigah T, Badel É, Cochard H, Herbette S (2010) Poplar vulnerability to xylem cavitation acclimates to drier soil conditions. Physiol Plant 139:280–288.

Barigah TS, Charrier O, Douris M, Bonhomme M, Herbette S, Améglio T, Fichot R, Brignolas F, Cochard H (2013) Water stress-induced xylem hydraulic failure is a causal factor of tree mortality in beech and poplar. Ann Bot 112:1431–1437.

Barigah TS, Ibrahim T, Bogard A, Faivre-Vuillin B, Lagneau LA, Montpied P, Dreyer E (2006) Irradiance-induced plasticity in the hydraulic properties of saplings of different temperate broad-leaved forest tree species. Tree Physiol 26:1505–1516.

Brodersen CR, Lee EF, Choat B, Jansen S, Phillips RJ, Shackel KA, McElrone AJ, Matthews MA (2011) Automated analysis of three-dimensional xylem networks using high-resolution computed tomography. New Phytol 191(4), 1168-1179.

Brodersen CR, McElrone AJ, Choat B, Lee EF, Shackel KA, Matthews MA (2013) In vivo visualizations of drought-induced embolism spread in *Vitis vinifera*. Plant Physiol 161(4): 1820-1829.

Cai J, Tyree MT (2010) The impact of vessel size on vulnerability curves: data and models for within-species variability in saplings of aspen, Populus tremuloides Michx. Plant Cell Env 33:1059–1069.

Carlquist S (1966) Wood Anatomy of Compositae: A Summary, With Comments on Factors Controlling Wood Evolution. Aliso: A Journal of Systematic and Evolutionary Botany 6:25–44.

634 Choat B, Cobb AR, Jansen S (2008) Structure and function of bordered pits: new discoveries
635 and impacts on whole-plant hydraulic function. New Phytol 177: 608–626.

636 Choat B, Jansen S, Brodribb TJ, Cochard H, Delzon S, Bhaskar R, Bucci SJ, Feild TS, Gleason
637 SM, Hacke UG, Jacobsen AL, Lens F, Maherali H, Martínez-Vilalta J, Mayr S,
638 Mencuccini M, Mitchell PJ, Nardini A, Pittermann J, Pratt RB, Sperry JS, Westoby M,
639 Wright IJ, Zanne AE (2012) Global convergence in the vulnerability of forests to
640 drought. Nature 491:752–755.

641 Choat B, Pittermann J (2009) New insights into bordered pit structure and cavitation resistance
642 in angiosperms and conifers. New Phytol 182: 557-560.

643 Christman MA, Sperry JS, Adler FR (2009) Testing the 'rare pit' hypothesis for xylem
644 cavitation resistance in three species of Acer. New Phytol 182:664–674.

645 Cochard H (2002) A technique for measuring xylem hydraulic conductance under high negative
646 pressures. Plant Cell Env 25:815–819.

647 Cochard H, Badel E, Herbette S, Delzon S, Choat B, Jansen S (2013) Methods for measuring
648 plant vulnerability to cavitation: a critical review. J Exp Bot 64:4779–4791.

649 Cochard H, Damour G, Bodet C, Tharwat I, Poirier M, Améglio T (2005) Evaluation of a new
650 centrifuge technique for rapid generation of xylem vulnerability curves. Physiol Plant
651 124:410–418.

652 Cochard H, Delzon S, Badel É (2015) X-ray microtomography (micro-CT): a reference
653 technology for high-resolution quantification of xylem embolism in trees. Plant Cell
654 Env 38:201–206.

655 Cochard H, Hölttä T, Herbette S, Delzon S, Mencuccini M (2009) New insights into the
656 mechanisms of water-stress-induced cavitation in conifers. Plant Physiol 151:949–954.

657 Cohen S, Bennink J, Tyree M (2003) Air method measurements of apple vessel length
658 distributions with improved apparatus and theory. J Exp Bot 54:1889–1897.

659 Cooke JEK, Martin TA, Davis JM (2005) Short-term physiological and developmental
660 responses to nitrogen availability in hybrid poplar. New Phytol 167:41–52.

661 De Rybel B, Mähönen AP, Helariutta Y, Weijers D (2016) Plant vascular development: from
662 early specification to differentiation. Nat Rev Mol Cell Biol 17:30–40.

663 Domec J-C, Gartner BL (2001) Cavitation and water storage capacity in bole xylem segments
664 of mature and young Douglas-fir trees. Trees 15:204–214.

665 Ewers FW, Ewers JM, Jacobsen AL, López-Portillo J (2007) Vessel redundancy: Modeling
666 safety in numbers. IAWA J 28:373–388.

667 Fichot R, Barigah TS, Chamaillard S, Le Thiec D, Laurans F, Cochard H, Brignolas F (2010)
668 Common trade-offs between xylem resistance to cavitation and other physiological
669 traits do not hold among unrelated Populus deltoides ×Populus nigra hybrids. Plant Cell
670 Env 33:1553–1568.

671 Gleason SM, Westoby M, Jansen S, Choat B, Hacke UG, Pratt RB, Bhaskar R, Brodribb TJ,
672 Bucci SJ, Cao K-F, Cochard H, Delzon S, Domec J-C, Fan Z-X, Feild TS, Jacobsen AL,
673 Johnson DM, Lens F, Maherali H, Martínez-Vilalta J, Mayr S, McCulloh KA,
674 Mencuccini M, Mitchell PJ, Morris H, Nardini A, Pittermann J, Plavcová L, Schreiber
675 SG, Sperry JS, Wright IJ, Zanne AE (2016) Weak tradeoff between xylem safety and
676 xylem-specific hydraulic efficiency across the world's woody plant species. New Phytol
677 209:123–136.

678 Hacke UG, Sperry JS, Wheeler JK, Castro L (2006) Scaling of angiosperm xylem structure
679 with safety and efficiency. Tree Physiol 26: 689–701.

680 Hajek P, Leuschner C, Hertel D, Delzon S, Schuldt B (2014) Trade-offs between xylem
681 hydraulic properties, wood anatomy and yield in *Populus*. Tree Physiol 34:744–756.

682 Hammond WM, Yu K, Wilson LA, Will RE, Anderegg WRL, Adams HD (2019) Dead or
683 dying? Quantifying the point of no return from hydraulic failure in drought-induced tree
684 mortality. New Phytol 223:1834–1843.

685 Hartmann H, McDowell NG, Trumbore S (2015) Allocation to carbon storage pools in Norway
686 spruce saplings under drought and low CO2. Tree Physiol 35:243–252.

687 Herbette S, Bouchet B, Brunel N, Bonnin E, Cochard H, Guillon F (2015) Immunolabelling of
688 intervessel pits for polysaccharides and lignin helps in understanding their hydraulic
689 properties in Populus tremula × alba. Ann Bot 115:187–199.

690 Herbette S, Cochard H (2010) Calcium Is a Major Determinant of Xylem Vulnerability to
691 Cavitation. Plant Physiol 153:1932–1939.

692 Herbette S, Wortemann R, Awad H, Huc R, Cochard H, Barigah TS (2010) Insights into xylem
693 vulnerability to cavitation in Fagus sylvatica L.: phenotypic and environmental sources
694 of variability. Tree Physiol 30:1448–1455.

695 Jacobsen AL, Pratt RB, Venturas MD, Hacke UG (2019) Large volume vessels are vulnerable
696 to water-stress-induced embolism in stems of poplar. IAWA J 40: 4-22.

697 Jansen S, Klepsch M, Li S, Kotowska M, Schiele S, Zhang Y, Schenk H (2018) Challenges in
698 understanding air-seeding in angiosperm xylem. Acta Hort 1222: 13-20.

699 Jansen S, Choat B, Pletsers A (2009) Morphological variation of intervessel pit membranes and
700 implications to xylem function in angiosperms. Am J Bot 96:409–419.

701 Jinagool W, Lamacque L, Delmas M, Delzon S, Cochard H, Herbette S (2018) Is there
702 variability for xylem vulnerability to cavitation in walnut tree cultivars and species
703 (Juglans spp.)? HortSci 53:132–137.

704 Jinagool W, Rattanawong R, Sangsing K, Barigah TS, Gay F, Cochard H, Kasemsap P,
705 Herbette S (2015) Clonal variability for vulnerability to cavitation and other drought-
706 related traits in Hevea brasiliensis Müll. Arg. J Plant Hydraul 2:e001.

707 Kaack L, Altaner CM, Carmesin C, Diaz A, Holler M, Kranz C, Neusser G, Odstrcil M, Schenk
708 HJ, Schmidt V, Weber M, Zhang Y, Jansen S (2019) Function and three-dimensional
709 structure of intervessel pit membranes in angiosperms: a review. IAWA J 40:673–702.

710 Kaack L, Weber M, Isasa E, Karimi Z, Li S, Pereira L, Trabi CL, Zhang Y, Schenk HJ, Schuldt
711 B, Schmidt V, Jansen S (2020) Pore constrictions in intervessel pit membranes reduce
712 the risk of embolism spreading in angiosperm xylem. bioRxiv:345413.

713 Klepsch MM, Schmitt M, Paul Knox J, Jansen S (2016) The chemical identity of intervessel pit
714 membranes in Acer challenges hydrogel control of xylem hydraulic conductivity. AoB
715 PLANTS 8: plw052.

716 Klepsch M, Zhang Y, Kotowska MM, Lamarque LJ, Nolf M, Schuldt B, Torres-Ruiz JM, Qin
717 D-W, Choat B, Delzon S, Scoffoni C, Cao K-F, Jansen S (2018) Is xylem of angiosperm
718 leaves less resistant to embolism than branches? Insights from microCT, hydraulics, and
719 anatomy. J Exp Bot 69:5611–5623.

720 Knipfer T, Brodersen CR, Zedan A, Kluepfel DA, McElrone AJ (2015) Patterns of drought-
721 induced embolism formation and spread in living walnut saplings visualized using X-
722 ray microtomography. Tree Physiol 35: 744-755.

723 Knipfer T, Cuneo IF, Brodersen CR, McElrone AJ (2016) In situ visualization of the dynamics
724 in xylem embolism formation and removal in the absence of root pressure: a study on
725 excised grapevine stems. Plant Physiol 171(2), 1024-1036.

726 Lamy J-B, Bouffier L, Burlett R, Plomion C, Cochard H, Delzon S (2011) Uniform selection
727 as a primary force reducing population genetic differentiation of cavitation resistance
728 across a species range. PLOS ONE 6:e23476.

729 Lamy J-B, Plomion C, Kremer A, Delzon S (2012) QST < FST As a signature of canalization.
730 Mol Ecol 21:5646–5655.

731 Lens F, Sperry JS, Christman MA, Choat B, Rabaey D, Jansen S (2011) Testing hypotheses
732 that link wood anatomy to cavitation resistance and hydraulic conductivity in the genus
733 Acer. New Phytol 190:709–723.

734 Lens F, Tixier A, Cochard H, Sperry JS, Jansen S, Herbette S (2013) Embolism resistance as a
735 key mechanism to understand adaptive plant strategies. Cur Op Plant Biol 16:287–292.

736 Li S, Lens F, Espino S, Karimi Z, Klepsch M, Schenk HJ, Schmitt M, Schuldt B, Jansen S
737 (2016) Intervessel pit membrane thickness as a key determinant of embolism resistance
738 in angiosperm xylem. IAWA J 37:152–171.

739 Loepfe L, Martinez-Vilalta J, Pinol J, Mencuccini M (2017) The relevance of the xylem
740 network structure for plant hydraulic efficiency and safety. J Th Biol 247: 788-803.

741 Maherali H, Moura CF, Caldeira MC, Willson CJ, Jackson RB (2006) Functional coordination
742 between leaf gas exchange and vulnerability to xylem cavitation in temperate forest
743 trees. Plant Cell Env 29:571–583.

744 Martínez-Vilalta J, Cochard H, Mencuccini M, Sterck F, Herrero A, Korhonen JFJ, Llorens P,
745 Nikinmaa E, Nolè A, Poyatos R, Ripullone F, Sass-Klaassen U, Zweifel R (2009)
746 Hydraulic adjustment of Scots pine across Europe. New Phytol 184:353–364.

747 Melcher PJ, Zwieniecki MA, Holbrook NM (2003) Vulnerability of xylem vessels to cavitation
748 in sugar maple. Scaling from individual vessels to whole branches. Plant Physiol 131(4):

749 1775-1780.

750 Mrad A, Domec JC, Huang CW, Lens F, Katul G (2018) A network model links wood anatomy
751 to xylem tissue hydraulic behaviour and vulnerability to cavitation. Plant Cell Env
752 41:2718-2730.

753 Niez B, Dlouha J, Moulia B, Badel É (2019) Water-stressed or not, the mechanical acclimation
754 is a priority requirement for trees. Trees 33:279–291.

755 Pammenter NW, Van der Willigen C (1998) A mathematical and statistical analysis of the
756 curves illustrating vulnerability of xylem to cavitation. Tree Physiol 18:589–593.

757 Pereira L, Flores-Borges DNA, Bittencourt PRL, Mayer JLS, Kiyota E, Araújo P, Jansen S,
758 Freitas RO, Oliveira RS, Mazzafera P (2018) Infrared nanospectroscopy reveals the
759 chemical nature of pit membranes in water-conducting cells of the plant xylem. Plant
760 Physiol 177:1629–1638.

761 Plavcová L, Hacke UG (2012) Phenotypic and developmental plasticity of xylem in hybrid
762 poplar saplings subjected to experimental drought, nitrogen fertilization, and shading. J
763 Exp Bot 63:6481–6491.

764 Plavcová L, Hacke UG, Sperry JS (2011) Linking irradiance-induced changes in pit membrane
765 ultrastructure with xylem vulnerability to cavitation. Plant Cell Env 34:501–513.

766 Plavcová L, Jansen S, Klepsch M, Hacke UG (2013) Nobody's perfect: can irregularities in pit
767 structure influence vulnerability to cavitation? Front Plant Sci 4: 453.

768 Schenk HJ, Espino S, Romo DM, Nima N, Do AYT, Michaud JM, Papahadjopoulos-Sternberg
769 B, Yang J, Zuo YY, Steppe K, Jansen S (2017) Xylem surfactants introduce a new
770 element to the cohesion-tension theory. Plant Physiol 173:1177–1196.

771 Schenk, H. J., Espino, S., Rich-Cavazos, S. M., & Jansen, S. (2018). From the sap's perspective:
772 the nature of vessel surfaces in angiosperm xylem. Am J Bot 105:174-187.

773 Schindelin J, Arganda-Carreras I, Frise E, Kaynig V, Longair M, Pietzsch T, Preibisch S,
774 Rueden C, Saalfeld S, Schmid B, Tinevez J-Y, White DJ, Hartenstein V, Eliceiri K,
775 Tomancak P, Cardona A (2012) Fiji: an open-source platform for biological-image
776 analysis. Nature Methods 9:676–682.

777 Schneider CA, Rasband WS, Eliceiri KW (2012) NIH Image to ImageJ: 25 years of image
778 analysis. Nature Methods 9:671–675.

779 Scholander PF, Bradstreet ED, Hemmingsen EA, Hammel HT (1965) Sap pressure in vascular
780 plants: Negative hydrostatic pressure can be measured in plants. Sci 148:339–346.

781 Scholz A, Klepsch M, Karimi Z, Jansen S (2013b) How to quantify conduits in wood? Front
782 Plant Sci 4:56.

783 Scholz A, Rabaey D, Stein A, Cochard H, Smets E, Jansen S (2013a) The evolution and function
784 of vessel and pit characters with respect to cavitation resistance across 10 Prunus
785 species. Tree Physiol 33:684–694.

786 Schuldt B, Knutzen F, Delzon S, Jansen S, Müller-Haubold H, Burlett R, Clough Y, Leuschner
787 C (2016) How adaptable is the hydraulic system of European beech in the face of climate
788 change-related precipitation reduction? New Phytol 210:443–458.

789 Sperry JS, Hacke UG, Wheeler JK (2005) Comparative analysis of end wall resistivity in xylem
790 conduits. Plant Cell Env 28:456–465.

791 Steudle E (2001) The cohesion-tension mechanism and the acquisition of water by plant roots.
792 Ann Rev Plant Physiol Plant Molecul Biol 52:847–875.

793 Taylor-Teeples M, Lin L, Lucas M de, Turco G, Toal TW, Gaudinier A, Young NF, Trabucco
794 GM, Veling MT, Lamothe R, Handakumbura PP, Xiong G, Wang C, Corwin J,
795 Tsoukalas A, Zhang L, Ware D, Pauly M, Kliebenstein DJ, Dehesh K, Tagkopoulos I,
796 Breton G, Pruneda-Paz JL, Ahnert SE, Kay SA, Hazen SP, Brady SM (2015) An
797 Arabidopsis gene regulatory network for secondary cell wall synthesis. Nature 517:571–
798 575.

799 Tixier A, Herbette S, Jansen S, Capron M, Tordjeman P, Cochard H, Badel É (2014) Modelling
800 the mechanical behaviour of pit membranes in bordered pits with respect to cavitation
801 resistance in angiosperms. Ann Bot 114:325–334.

802 Torres-Ruiz J.M., Cochard H., Mencuccini M., Delzon S., Badel E. 2016. Direct observations
803 and modelling of embolism spread between xylem conduits: a case study in Scot pine.
804 Plant Cell Env 39:2774-2785.

805 Tyree MT, Davis SD, Cochard H (1994) Biophysical perspectives of xylem evolution: is there
806 a tradeoff of hydraulic efficiency for vulnerability to dysfunction? IAWA J 15:335–360.

807 Wheeler JK, Sperry JS, Hacke UG, Hoang N (2005) Inter-vessel pitting and cavitation in woody
808 Rosaceae and other vesselled plants: a basis for a safety versus efficiency trade-off in
809 xylem transport. Plant Cell Env 28:800–812.

810 Wortemann R, Herbette S, Barigah TS, Fumanal B, Alia R, Ducousso A, Gomory D, Roeckel-
811 Drevet P, Cochard H (2011) Genotypic variability and phenotypic plasticity of
812 cavitation resistance in Fagus sylvatica L. across Europe. Tree Physiol 31:1175–1182.

813 Zimmermann MH, Jeje AA (1981) Vessel-length distribution in stems of some American
814 woody plants. Can J Bot 59:1882–1892.

815 Zhang Y, Carmesin C, Kaack L, Klepsch MM, Kotowska M, Matei T, Schenk HJ, Weber M,
816 Walther P, Schmidt V, Jansen S (2020) High porosity with tiny pore constrictions and
817 unbending pathways characterize the 3D structure of intervessel pit membranes in
818 angiosperm xylem. Plant Cell Env 43:116–130.

Figure 1: Measurement of the embolism pressure (P_e) of each individual vessel. A-D: Direct observation of embolism spread using a x-ray microtomograph in an intact xylem stem under increasing tension. Black areas reveal the embolized vessels. A: native state (Ψ = 0 MPa). B: Ψ = - 1.5 MPa. C: P_{50} state (Ψ = - 2.5 MPa). D: final state (Ψ = - 4 MPa). E: Cut of the same stem sample observed using light microscopy. The resulting image resolution allows us measuring accurately the anatomical traits. Colour represents the embolism pressure (P_e) of each vessel, as measured with x-ray microtomography. Shown images are from a subset of approx. 230 vessels on a control plant.

Figure 2: Xylem hydraulic traits in trees depending on the growth conditions. A: Xylem vulnerability curve. Each line is the mean curve per condition: droughted, n = 9 from 9 trees; control, n = 10 from 5 trees; shaded, n = 12 from 6 trees. Dashed line, droughted plants; full line, control plants; dotted line, shaded plants. Grey areas represent the standard deviations around the means. Horizontal dotted line indicates the 50 % loss of conductance. B: Hydraulic specific conductivity (K_s). Data are mean values for 8 droughted trees, 9 control trees, 9 shaded trees. Error bars show the standard deviation.

Figure 3: Correlation between P_{50} and several xylem structural traits. Data are squares of the coefficient of correlation (R^2) for each factor with P_{50}. Black bars indicate pit-related traits and white bars indicate vessel and xylem-related traits. On the x-axis, a "+" symbol indicates a positive correlation, while a "-" symbol indicates a negative one. Stars indicate the significance of the correlation: "***", $p < 0.001$; "**", $0.001 < p < 0.01$; "ns", non-significant correlation.

Figure 4: Correlation between P_{50} and two xylem structural traits. A: Relationship between P_{50} and pit area per vessel (A_p). B: Relationship between P_{50} and vessel grouping index (GI). Each

844 point represents the mean value for an individual tree. Black circles refer to droughted plants;
845 white circles refer to control plants and white squares refer to shaded plants. The dotted line is
846 the regression line.
847
848 Figure 5: Correlation between P_e and vessel traits within xylem. Data are all vessel
849 measurements pooled from analyses on four individuals using X-ray microtomography. A-C:
850 Vulnerability to embolism curves of vessels grouped by classes depending on structural traits.
851 A: Vessels clustered by diameter (D_v^*) classes. The dash sizes of the lines indicate the vessel
852 diameter class: from full line (narrow vessels) to dotted line (wide vessels). B: Vessels clustered
853 by classes for fraction of membrane length in contact with other vessels (F_c^*). The dash sizes
854 of the lines indicate the vessel contact fraction class: from full line (non-contact vessels) to
855 dotted line (vessels sharing high portion of membrane length). C: Vessels are clustered by group
856 size (GS) classes. The dash sizes of the lines indicate the vessel group sizes: from full line
857 (solitary vessels) to dotted line (vessels in large groups). D: Vessels clustered by distance from
858 the pith. The relative distance is between 0 and 1, 0 being close to the pith. The dash sizes of
859 the lines indicate the vessel distance class: from full line (vessels close to the pith) to dotted line
860 (vessels far from the pith).
861 Figure 6: Correlation between P_e and xylem traits. Data are squares of the coefficient of
862 correlation (R^2) for each factor with P_e. On the x-axis, a "+" symbol indicates a positive
863 correlation, while a "-" symbol indicates a negative one. Stars indicate the significance of the
864 correlation for the trait: "***", $p < 0.001$.

Table 1: Meanings of the symbols.

Symbol	Definition	Unit
Ψ_{pd}	Predawn water potential	MPa
Ψ_{md}	Midday water potential	MPa
LA	Mean leaf area	cm^2
A_p	Mean total pit area per vessel	mm^2
A_v	Mean area per vessel	mm^2
D_a	Mean pit aperture diameter	µm
D_p	Mean pit diameter	µm
D_v	Mean vessel diameter	µm
D_v^*	Vessel diameter	µm
F_c	Mean contact fraction: mean membrane length in contact with other vessels over total membrane length	%
F_c^*	Vessel contact fraction: for each vessel, fraction of membrane length in contact with other vessels	%
F_p	Mean pit fraction: mean total pit area in contact with other vessels over total vessel area	%
F_{pf}	Mean pit-field fraction: pit area over inter-vessel area	%
GI	Vessel grouping index	-
GS	Vessel group size	-
K_{s_theo}	Theoretical hydraulic conductivity	$kg.s^{-1}.MPa^{-1}.m^{-1}$
K_s	Specific hydraulic conductivity	$kg.s^{-1}.MPa^{-1}.m^{-1}$
L_p	Mean pit chamber depth	µm
L_v	Median vessel length	µm
P_{50}, P_{12}, P_{88}	Pressure inducing 50, 12, 88 % loss of xylem conductance	MPa
P_e	Pressure inducing embolism in a vessel	MPa
SI	Vessel solitary index	%
T_m	Mean pit membrane thickness	µm

Table 2: Physiological characterisation of sapling grown under the three different conditions.

Factor	Unit	Droughted	Control	Shaded
Ψ_{pd} m-1	Mpa	- 0.22 ± 0.12 [a]	- 0.11 ± 0.04 [b]	- 0.13 ± 0.01 [b]
Ψ_{md} m-1	MPa	- 0.96 ± 0.15 [a]	- 0.69 ± 0.05 [b]	- 0.77 ± 0.09 [b]
Ψ_{pd} d-1	Mpa	- 0.59 ± 0.44 [a]	- 0.14 ± 0.03 [b]	- 0.11 ± 0.02 [b]
Ψ_{md} d-1	MPa	- 1.44 ± 0.33 [a]	- 0.98 ± 0.06 [b]	- 0.98 ± 0.11 [b]
LA	cm^2	87.64 ± 18.41 [a]	137.61 ± 17.55 [b]	184.13 ± 40.34 [c]
Height	Mm	1685 ± 187 [a]	2237 ± 263 [b]	2282 ± 76 [b]
Diameter	Mm	9.47 ± 0.83 [a]	13.96 ± 0.49 [b]	10.94 ± 0.61 [b]
K_{s_theo}	$kg.s^{-1}.MPa^{-1}.m^{-1}$	0.949 ± 0.336 [a]	1.380 ± 0.274 [b]	1.405 ± 0.198 [b]
K_s	$kg.s^{-1}.MPa^{-1}.m^{-1}$	1.054 ± 0.192 [a]	1.043 ± 0.301 [a]	0.954 ± 0.330 [a]
P_{50}	MPa	- 3.03 ± 0.23 [a]	- 2.49 ± 0.10 [b]	- 2.27 ± 0.18 [b]
P_{12}	MPa	- 2.55 ± 0.34 [a]	- 2.02 ± 0.11 [b]	- 1.87 ± 0.11 [b]
P_{88}	MPa	- 3.51 ± 0.24 [a]	- 2.95 ± 0.11 [b]	- 2.68 ± 0.11 [b]
Native Embolism	%	1.81 ± 10.47 [a]	- 7.48 ± 7.91 [ab]	- 10.81 ± 7.84 [b]

Data are mean values ± standard deviation for each growth condition. For each line, values not followed by the same letter differ significantly at $p < 0.05$ (one-way ANOVA). Water potentials (Ψ_{pd} and Ψ_{md}) were measured one month before (m-1) and the day before (d-1) stem sampling for hydraulic and structural analysis. Ψ_{pd}, Predawn water potential; Ψ_{md}, Midday water potential; LA, Leaf area; K_{s_theo}, Theoretical hydraulic conductivity; K_s, Specific hydraulic conductivity; P_{50}; P_{12}; P_{88}, pressure inducing 50; 12 and 88 percent loss of conductance.

Table 3: Xylem structural traits depending on the growth conditions.

Trait	Unit	Droughted	Control	Shaded
A_p	mm^2	1.20 ± 0.51^a	2.94 ± 0.65^b	3.78 ± 0.27^c
A_v	mm^2	8.21 ± 3.93^a	20.63 ± 3.64^b	26.65 ± 8.22^b
D_a	µm	3.67 ± 0.34	3.37 ± 0.61	3.98 ± 0.81
D_p	µm	9.18 ± 0.69	8.64 ± 0.55	8.89 ± 0.72
D_v	µm	31.22 ± 6.14^a	40.07 ± 1.98^b	42.71 ± 2.28^b
F_c	%	20.35 ± 2.70^a	19.01 ± 1.13^b	17.04 ± 0.96^c
F_p	%	15.95 ± 1.13^a	14.15 ± 0.77^b	12.53 ± 0.56^c
F_{pf}	%	74.45 ± 1.33	74.46 ± 2.93	74.13 ± 2.75
GI	-	1.84 ± 0.20^a	1.63 ± 0.05^b	1.51 ± 0.05^c
L_p	µm	1.99 ± 0.06	2.08 ± 0.03	1.87 ± 0.11
L_v	mm	70.79 ± 25.1^a	137.0 ± 18.86^b	164.6 ± 48.4^c
SI	%	33.13 ± 5.43^a	38.46 ± 2.19^b	43.73 ± 3.11^c
T_m	µm	0.26 ± 0.04	0.23 ± 0.04	0.24 ± 0.02

The meaning of the symbols is given in Table 1. For each trait, the method for measurement and number of replication are indicated in the methods section. Data are mean values ± standard deviation. For each line, values not followed by the same letter differ significantly at $p < 0.05$ (one-way ANOVA).

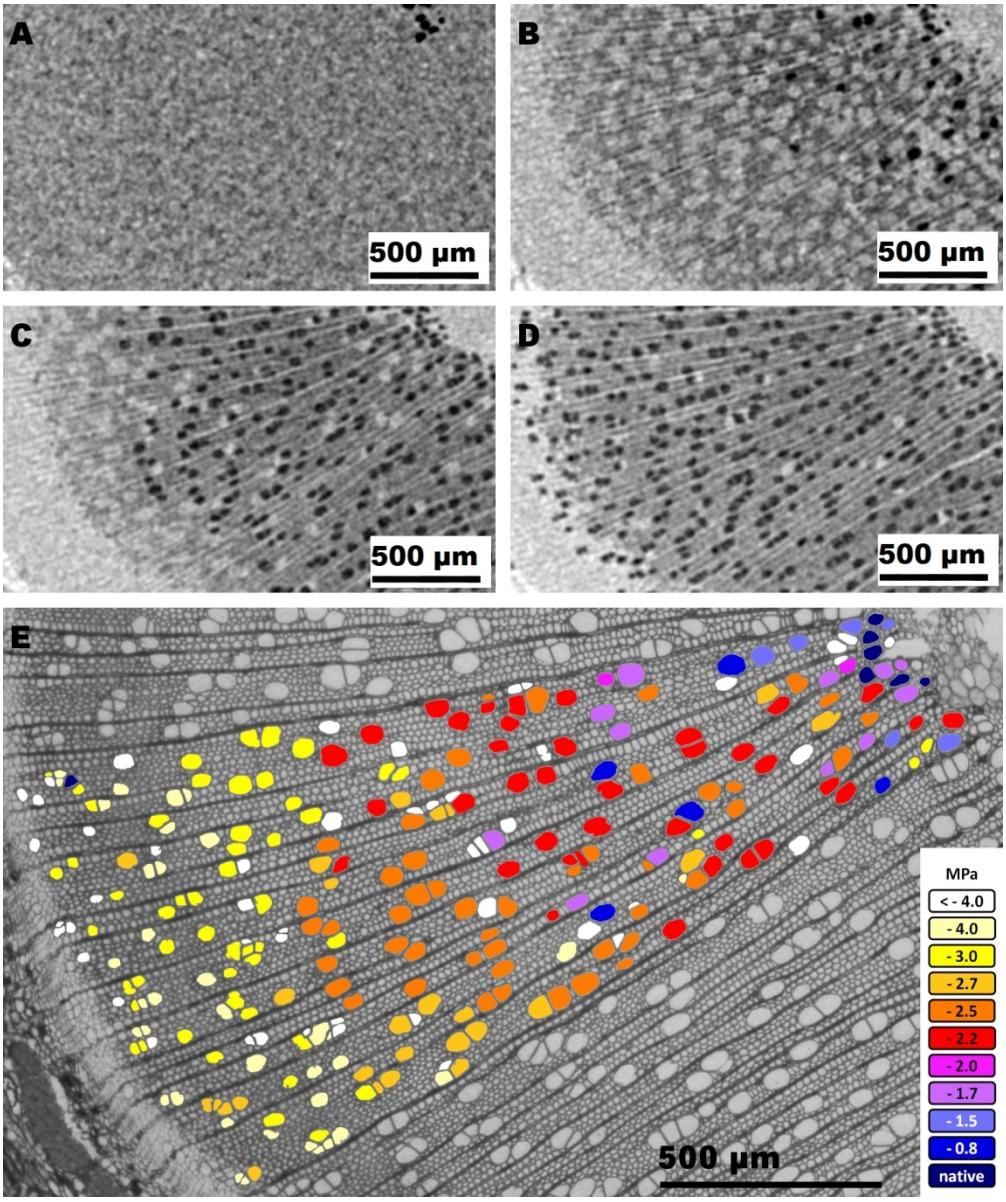

figure 1

339x404mm (120 x 120 DPI)

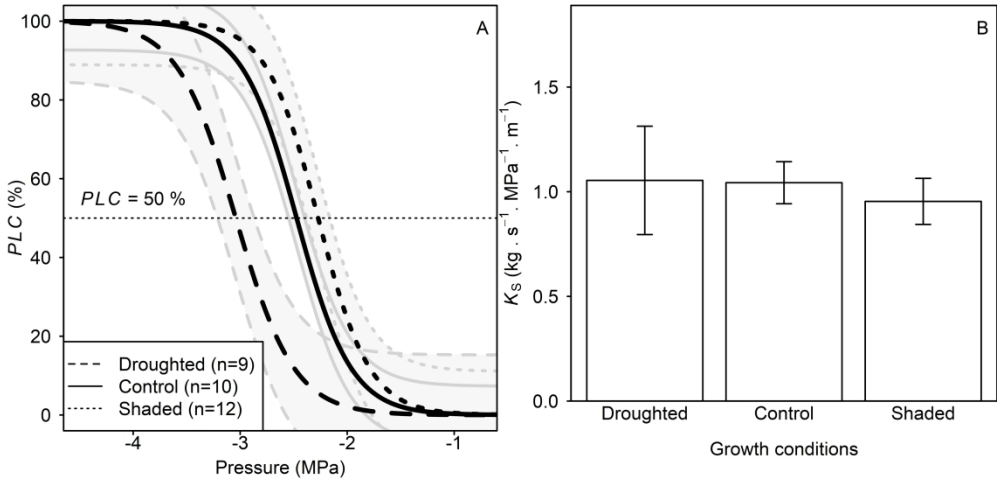

figure 2

171x82mm (600 x 600 DPI)

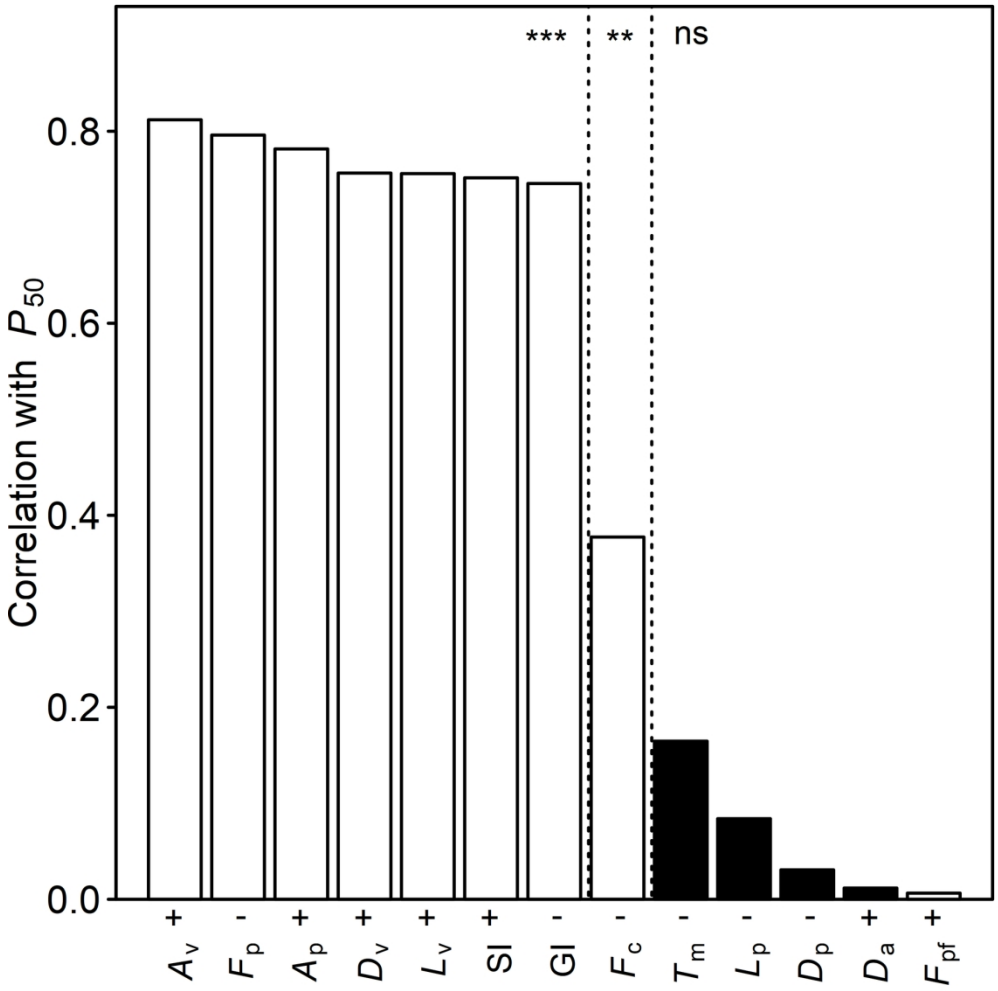

figure 3

82x82mm (600 x 600 DPI)

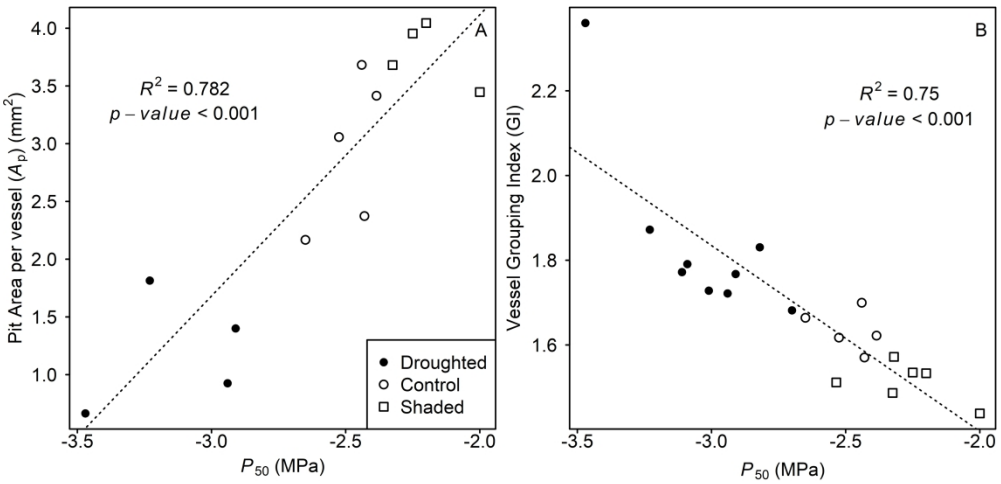

figure 4

171x82mm (600 x 600 DPI)

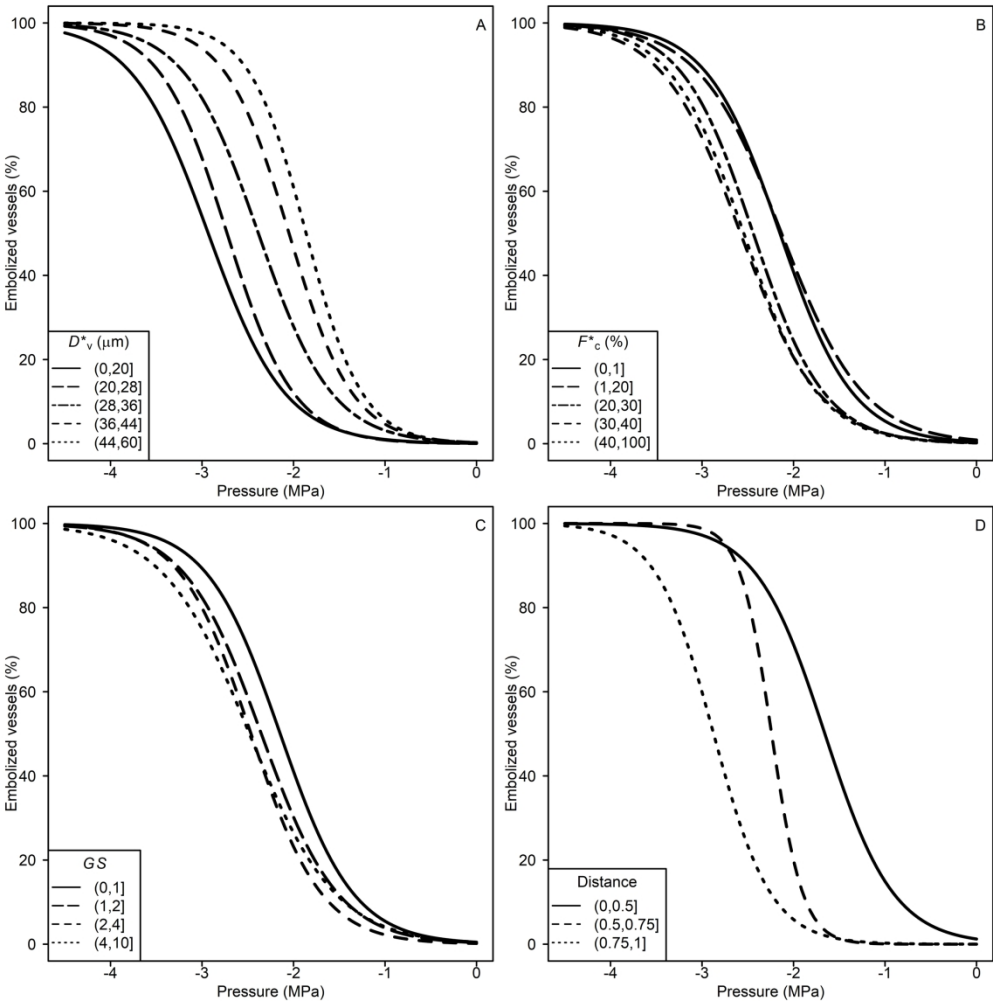

figure5

114x114mm (600 x 600 DPI)

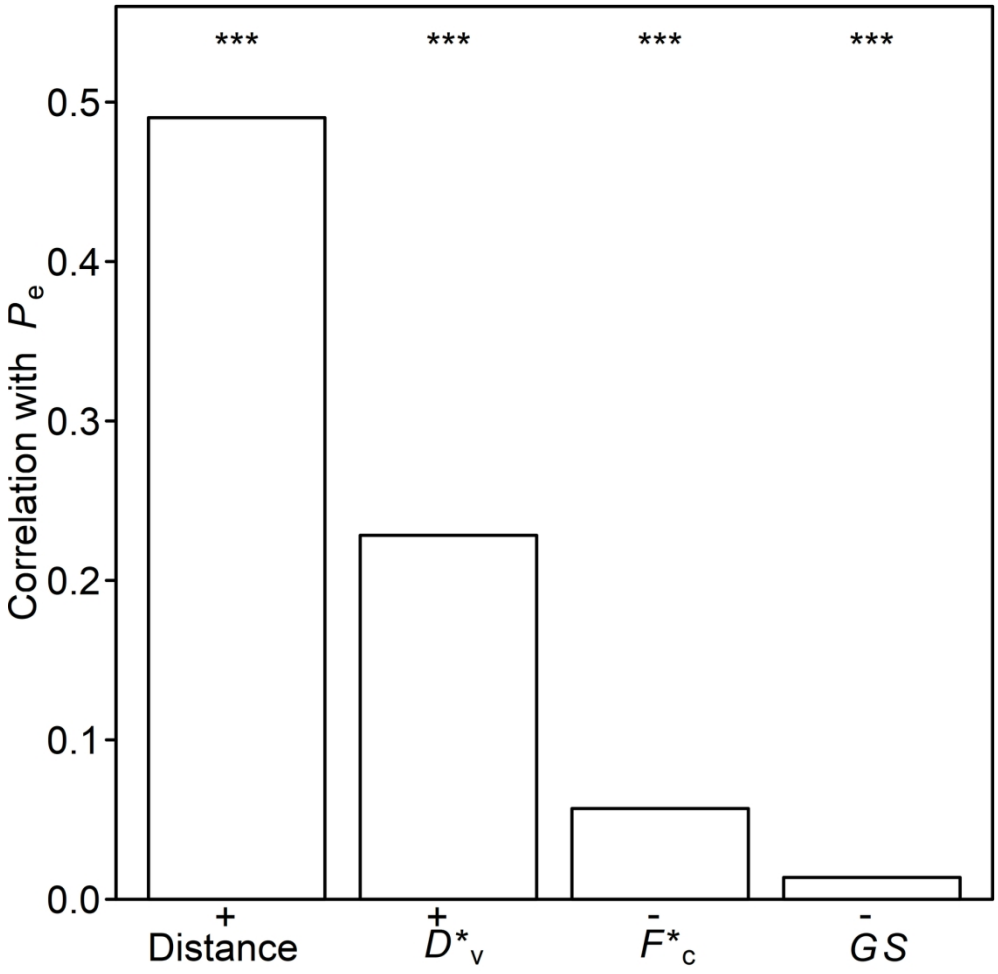

figure 6

82x82mm (600 x 600 DPI)